Available online at www.sciencedirect.com
SCIENCE DIRECT®
ELSEVIER
Journal of Nuclear Materials 322 (2003) 57–65
journal of nuclear materials
www.elsevier.com/locate/jnucmat

In situ crack growth observation and fracture toughness measurement of hydrogen charged Zircaloy-4

G. Bertolino [a,*], G. Meyer [a,b], J. Perez Ipiña [b,c]

[a] Centro Atómico Bariloche, CNEA, 8400 Bariloche, Argentina
[b] CONICET, National Council of Scientific and Technological Research, Argentina
[c] Universidad Nacional del Comahue, 8300 Neuquén, Argentina

Received 11 March 2003; accepted 17 June 2003

Abstract

The effect of hydrogen on the fracture behaviour of a Zircaloy-4 alloy was analysed performing simultaneous fracture mechanics tests of small SE(B) specimens and in situ observation of crack initiation and propagation inside the chamber of a scanning electron microscope. Load and displacement were continuously measured and J_{IC}, J–R curves and CTOD determinations were obtained. Detailed images of the zone close to the crack tip were taken and the resistance to crack growth was correlated with hydrogen content and hydride morphology. The size and orientation of hydride precipitates showed an important influence on the fracture process. A good agreement with results obtained using standard CT specimens was met.

1. Introduction

Zirconium (Zr) alloys are the major structural materials within the fuel region of a nuclear reactor. They are mainly used in the fuel cladding and fuel channel. During operation the working environment of these components is a combination of temperature and reactive conditions such as irradiation, oxidation and hydrogen (H) pick up. The hydrogen sources can be external, like H cathodically generated in the corrosion of the cladding by the primary side water coolant [1], radiolysis of the coolant water, the H gas dissolved in the primary side coolant in pressurized water reactors [2], or internal as the H contained in the fuel pellets [3]. At the temperature of reactor operation terminal solid solubility of hydrogen in Zr alloys is low (about 130 ppm-H wt at 623 K [4]) and further H absorption leads to the formation of zirconium hydrides. These hydrides are brittle and degrade the mechanical properties of the material. The two major embrittlement consequences of the H pick up are the reduction of both ductility and fracture toughness due to a high concentration of hydrides and, on the other hand, the subcritical crack growth called delayed hydride cracking (DHC) [5]. The extent of hydride embrittlement depends not only on the quantity of hydride phase, but also on the hydrides morphology and their orientation respect to the applied stress. Zirconium hydrides (ZrH) have received much attention as a fracture initiator because of their brittle behaviour and their thin platelet morphology of the δ phase [6]. The precipitate orientation is close related with the material texture and the stress state at the hydrides precipitation zone. In the case of pressure tubes, hydride orientation is mainly determined by the manufacturing process because it dominates the final texture and the grains shape and size [7].

The usual practice to characterise the fracture process consists of the measurement of fracture properties using adequate tests and the post-mortem analysis of the

* Corresponding author. Present address: LMS, UMR-CNRS, Ecole Polytechnique, 91128 Palaiseau cedex, France. Tel.: +33-169 333305; fax: +33-169 333507.
E-mail addresses: bertolin@cab.cnea.gov.ar, bertolin@lms.polytechnique.fr (G. Bertolino).

0022-3115/$ - see front matter © 2003 Elsevier B.V. All rights reserved.
doi:10.1016/S0022-3115(03)00305-2

fracture surfaces to identify the micro-mechanisms involved in the crack growth. It has been shown that the simultaneous measurement of fracture toughness parameters and the observation of the evolution of crack path provide valuable information to study complex material systems, i.e., multiphase materials, composites, etc. [8,9].

A study of the dependence of the fracture toughness of H charged Zircaloy-4 (Zry-4) with H content and the observation of the dominant mechanisms during crack propagation by means of in situ tests in the chamber of a scanning electron microscope (SEM) are presented in this work.

2. Experimental procedure

2.1. Material and specimens

Specimens were obtained from a Zry-4 rolled commercial plate 6 mm thick. The plate fabrication process included hot-rolling, cold-rolling, annealing and conditioning. The main alloying elements and impurities obtained by chemical analysis are shown in Table 1. The final material microstructure was α-Zry-4 fine equiaxed grains with a mean diameter of approximately 8 μm, Fig. 1. Laminated Zry shows an anisotropic mechanical behaviour caused by its characteristic texture [10]. Measurement of material texture showed that the *c*-axis was concentrated in the normal-transverse plane with maximums at 0° and 36° from the normal. Table 2 presents the main mechanical properties: ultimate tensile stress (σ_{UTS}), yield stress (σ_{ys}) and elongation ($\varepsilon\%$), measured at room temperature in the rolling and transverse directions.

The tested specimens consisted of small single edge-notched and fatigue pre-cracked beams loaded in three point bending (SSE(B)), Fig. 2, with $W = 7$ mm, thickness between 2 and 3 mm and the other dimensions according to standards [11]. Specimens were machined in direction LT and TL. The fatigue pre-cracking process was performed in an MTS 810, servo-hydraulic test machine, using load ranges in accordance with the standard.

The specimens were hydrogen charged using an electrochemical technique and then annealed to ensure homogeneous hydride distribution. H charge was typically carried out at room temperature in a solution of 0.1 M KOH with a current density of 10 mA/cm^2 during a period of time determined by the desired final concentration. The annealing process was performed at 400 °C in Argon (hydrogen) atmosphere for lower (higher) final H content. Then, the specimens were slowly cooled in the furnace.

After hydrogen charge and before testing, specimen's surfaces were treated according to the features to be observed during the test. The different surface observations included: polished only, grain structure, hydride

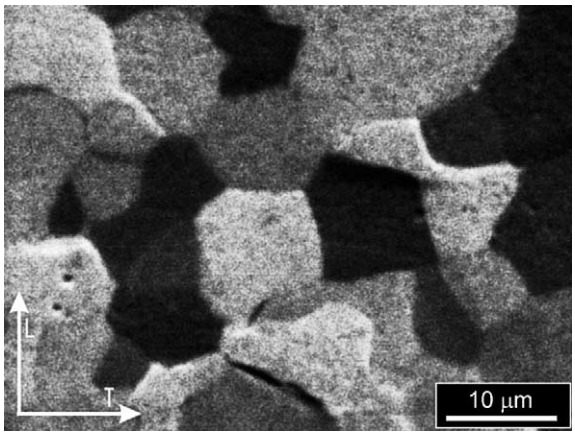

Fig. 1. Microstructure of α-Zry rounded grains of tested Zry-4.

Table 2
Basic mechanical properties at room temperature

Property	Longitudinal	Transversal
σ_{UTS} [MPa]	522	510
σ_{ys} [MPa]	365	460
$\varepsilon\%$	27.8	28.6

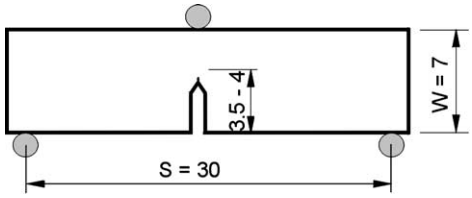

Fig. 2. Geometry of SSE(B) specimens (machined in the LT or TL directions).

Table 1
Chemical composition of used material

Alloying elements (wt%)					Main impurities (ppm)			
Fe	Cr	FeCr	S	O	Al	C	Hf	Si
0.21	0.1	0.31	1.42	0.125	25	110	52	39

distribution. In order to enhance grain boundaries, a chemical etching with a solution of glycerol, HNO_3, HF (in volumetric proportion of 10:9:1) was used; while an HNO_3–HF (23:2) solution was selected to reveal hydrides.

2.2. Fracture toughness testing

A small testing stage developed in Centro Atómico Bariloche (Argentina) was used to perform fracture mechanics tests [12]. It is a small double-screw device with an HBM ± 2 KN load cell and an HBM inductive displacement transducer WT 1 ± 1 mm to control and measure load and displacement values with a data acquisition board and a software developed in the laboratory. With this special device, mechanical tests based on a three point bend arrangement could be performed in the chamber of an SEM (PHILIPS 515). The selected procedure is similar to a conventional test: specimens were monotonically loaded while the applied load (P) and the load point displacement (v) were recorded. The loading process was stopped at regular steps and images were recorded. While in a conventional test, for example in the *Unloading Compliance* method, at each stop a partial unloading is performed to obtain the amount of crack growth, in this in situ test the growth is obtained directly by observation with SEM and any particular event observed in regions close to the crack tip can be correlated with the corresponding point in the load–displacement (P vs. v) record.

3. Results and discussion

This work introduces a study of the effect of hydrogen on the fracture toughness of Zry-4. Tests were performed in a small testing machine designed and built to be located inside an SEM chamber. The simultaneous observation of magnified images of crack initiation and propagation, and measurement of the load–displacement curves allow to relate micro-mechanisms acting during the crack growth process with the calculated fracture parameters.

H absorbed during charging formed precipitates of δ hydride phase in grain boundaries, platelet shaped, and oriented in planes parallel to the rolling direction. The distribution and size of hydrides are influenced by the cooling rate: whilst for fast cooling rates a homogeneous distribution of platelets is usually observed [13], for slow cooling rates the platelets are grouped in long bands. The latter was observed in this work, Fig. 3.

Stable crack growth was the feature in all the tests performed in this work, however, brittle behaviour was observed in macro-tests under conditions not evaluated here, i.e. H content greater than 1900 ppm and room temperature [14]. Fig. 4 shows a typical load–displacement record obtained in these in situ tests at room temperature. A load relaxation occurred at each loading stop, as can be observed in several points along the figure.

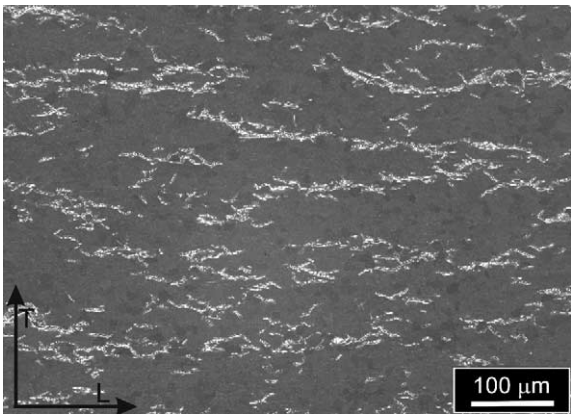

Fig. 3. Distribution of hydride platelets in long bands.

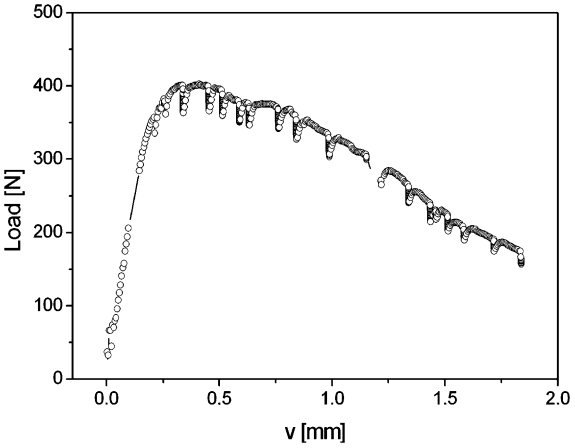

Fig. 4. Typical load–displacement curve.

It has been already shown that the elastic–plastic fracture mechanics is the appropriate technique to evaluate the toughness of Zry-4 [15]. A representative J–R curve is shown in Fig. 5 where SEM photographs were superimposed to the plot in order to compare J values with the crack tip profile evolution during the test. After the tests, the stable crack growth was marked in some specimens by heat-tinting to observe the crack front. The heat-tinting revealed that the crack front shape was nearly flat, which indicated that the crack length actually measured on the specimen surface was very close to the mean value.

Fig. 6 presents the J–R curves and the initiation values dependency with H content. These results were compared with J–R curves obtained testing conventional CT specimens ($W = 25.4$ mm) machined from the same

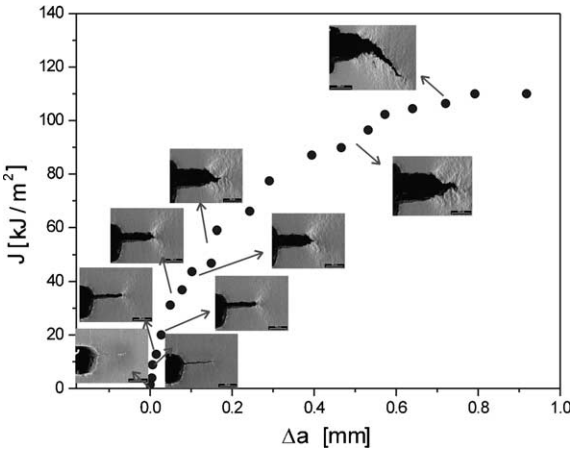

Fig. 5. J–R curve obtained from the P–v record of Fig. 4 ($J_{max} = 68$ kJ/m^2). Inserted pictures show different stages during crack growth.

material and with similar hydrogen content [14], Fig. 7. A good agreement was obtained between these two sets of results, but being the first ones a bit higher. This small difference could be explained considering the specimen size: the crack tip stress fields in the small samples are closer to the plane stress condition than to the plane strain one. Fig. 6(b) shows a reduction in J_{IC} values when H content increases, this behaviour was fitted with an exponential decay function. These results were also in agreement with those obtained testing macro-CT specimens.

Fig. 6(a) shows that the value of J at the point where the initiation of the propagation was detected is significantly lower than J_{IC} obtained following standard procedures [11]. The black circles in the curves indicate approximately the points where stable crack growth initiation was first observed. This discrepancy arises from the fact that J_{IC} is an engineering value obtained after a certain amount of crack growth (0.2 mm) so it

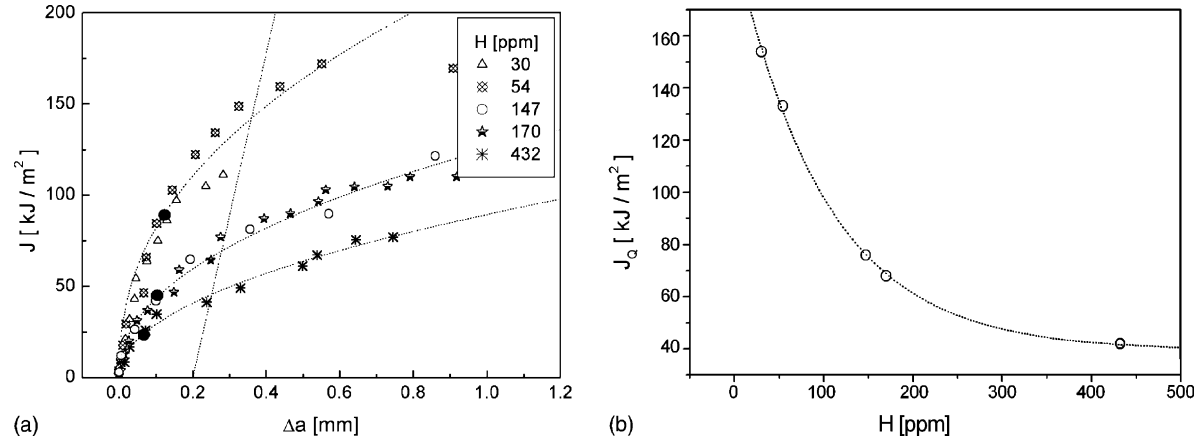

Fig. 6. (a) J–R curves at different H content and (b) J_{IC} vs. H curve.

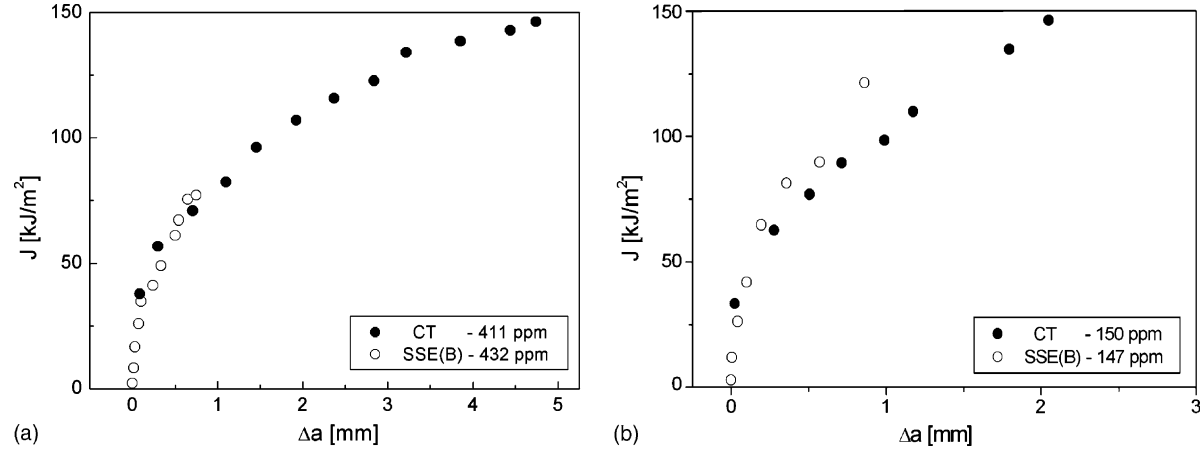

Fig. 7. Comparison of J–R curves for SSE(B) and CT specimens with similar H content.

must be always greater than J at the crack growth initiation.

To qualify the obtained results as *valid* according to ASTM standard [11], special attention must be paid to geometrical aspects of the sample. For employed SSE(B) specimens the limit for the stable crack growth ($\Delta a < 0.25 b_0$) was $\Delta a_{max} = 0.8$ mm. In the case of J, the limit is the lower value between $b\sigma_y/20$ or $B\sigma_y/20$, that resulted in a J_{max} of 68 (45) kJ/m^2 approximately for specimen with $B = 3$ (2) mm and the Zry-4 yield stress. Although the tests with low H did not fit previous conditions, their values were still useful to qualitatively understand the influence of H content on the material toughness.

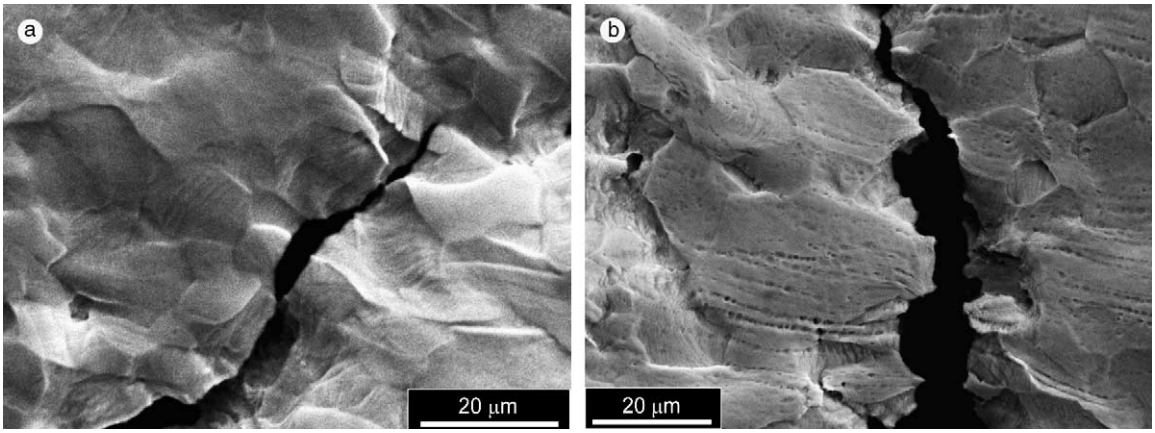

Fig. 8. Crack growth following: (a) transgranular and (b) intergranular paths.

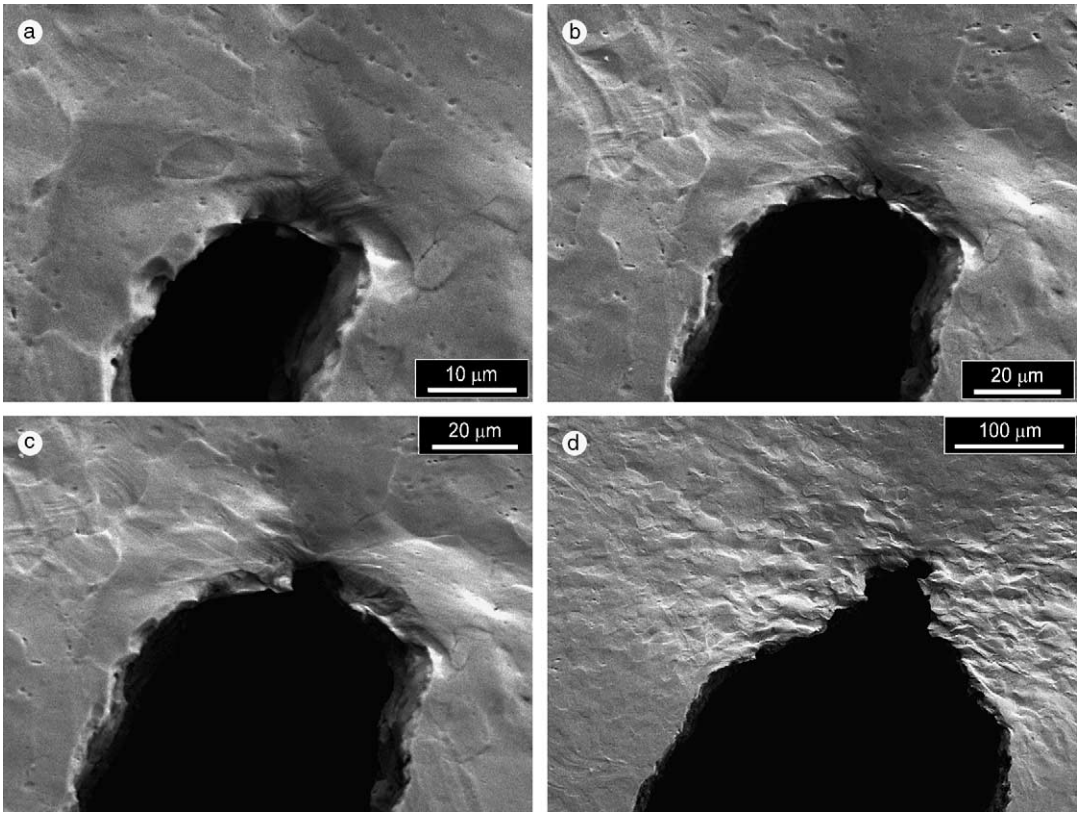

Fig. 9. Slow crack growth in an H uncharged specimen.

Different crack growth mechanisms were observed during the tests. Fig. 8 shows cracks following transgranular (a) and intergranular (b) paths in specimens with H content of 170 and 1300 ppm, respectively.

Fig. 9(a)–(d) shows the slow stable crack growth of a crack in an H uncharged specimen, with a typical ductile growth and blunting pattern. Fig. 10 shows the stable crack growth process in a specimen with medium hydrogen content involving less plastic deformation as well as a reduction of the blunting process. Fractured hydrides located ahead the crack tip were observed in almost all the specimens with medium to high hydrogen content, resulting a damaged zone around the crack path, Fig. 11. The observed behaviour confirms that the fracture micro-mechanisms acting during Zry-4 fracture were strongly dependent on H concentration and hy-

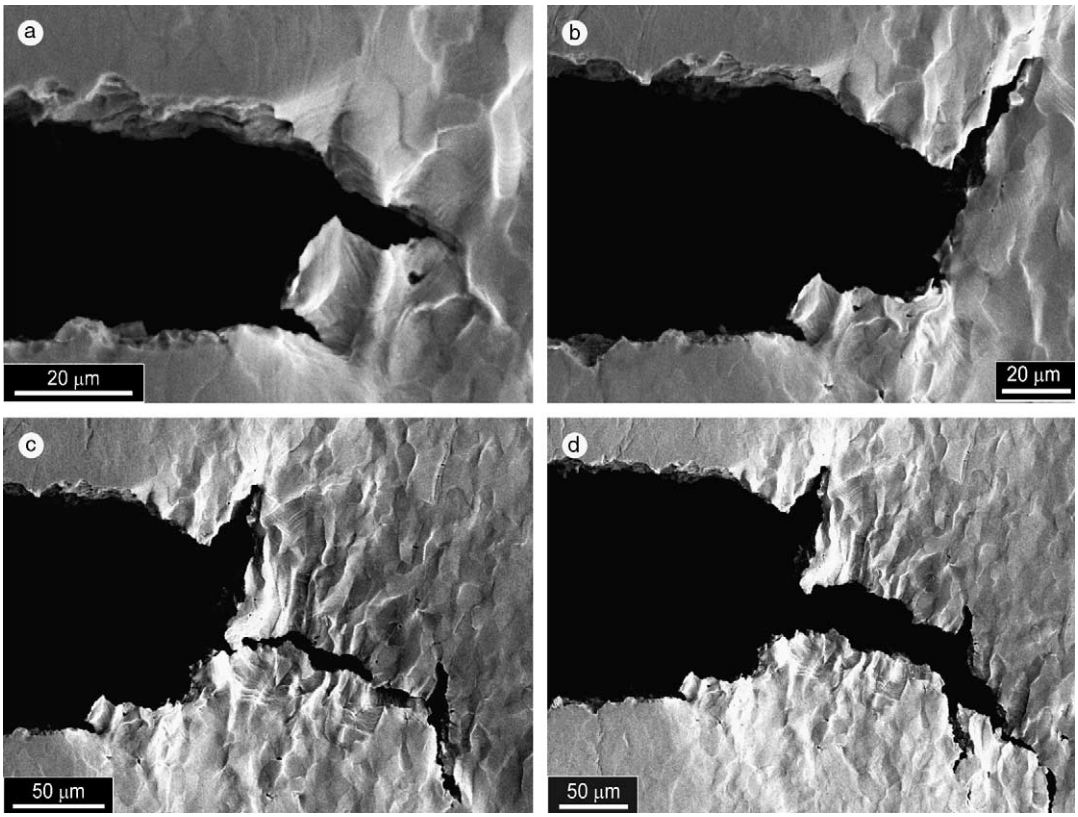

Fig. 10. Stable crack growth in a specimen with 600 ppm of H.

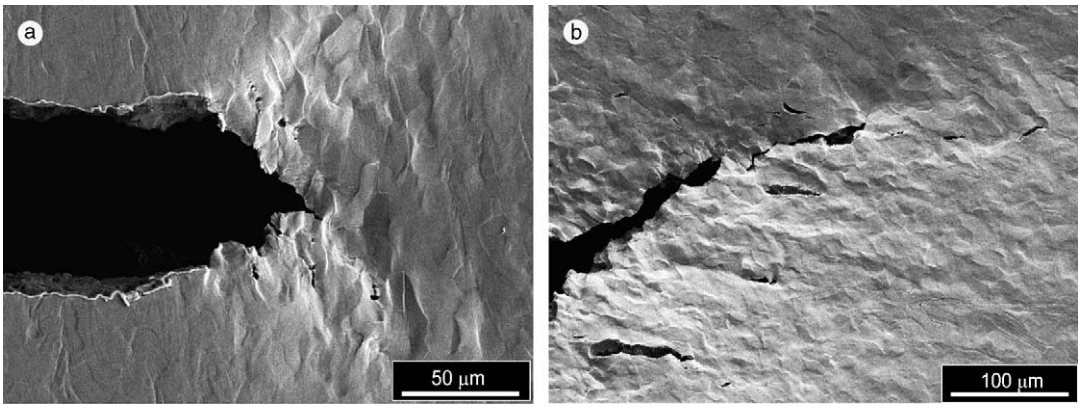

Fig. 11. Damaged zone ahead the crack tip in a specimen with 170 ppm of H.

dride orientation. At low H content and with small hydride precipitates, the fracture mode was ductile, Fig. 9(a). During crack growth a process involving crack blunting followed by a new crack tip development was alternatively observed. When the hydride phase precipitated as large platelets, they broke ahead of the crack tip and the final separation was by the ductile fracture of the matrix from the crack tip guided by the fractured hydrides, Fig. 9(b). At the higher H content, the precipitate size increased and both J_{IC} and the curve slope were reduced, Fig. 6.

When the notch was normal to the rolling direction, hydride precipitates were oriented normal to the crack. Precipitated hydrides ahead of the crack tip were fractured and the crack grew interconnecting them by ductile fracture of the matrix; thus a tortuous crack path was observed, Fig. 12. When the notch was parallel to the rolling direction, the precipitated hydrides were parallel to it, and the crack grew through them thus connecting the brittle hydrides and, therefore, involving less plastic deformation of the matrix, Fig. 13. Then, for the same H content, the fracture toughness was lower than that of hydrides normal to the crack, as can be seen in Fig. 14 where two crack tip open displacement (CTOD)-R curves of specimens with similar H content and both orientations are shown. The CTOD is another elastic–plastic fracture parameter related to J by $J = m\sigma_y$ CTOD (m is about 2 in plane strain conditions). It was determined in this work from the obtained photographs, by measuring the opening displacement of the initial crack tip on the specimen surface.

Only the phenomena occurring in the specimen surface can be observed with this methodology; which becomes a limitation, because the crack growth process is very often controlled by events inside the specimen volume.

Another remarkable aspect in this technique is, as can be observed in Figs. 3 and 12, that the hydrides are clearly identified on the specimen surface, therefore, when the crack grows during the test, the fracture path through the hydrides or the matrix can be followed. Instead, when the analysis is performed by observing a post-mortem fracture surface, the hydrides are not clearly identified, and their position is induced by the brittle appearance of some regions, under the supposition that the hydrides have fractured by cleavage while the matrix has done so in a ductile mode.

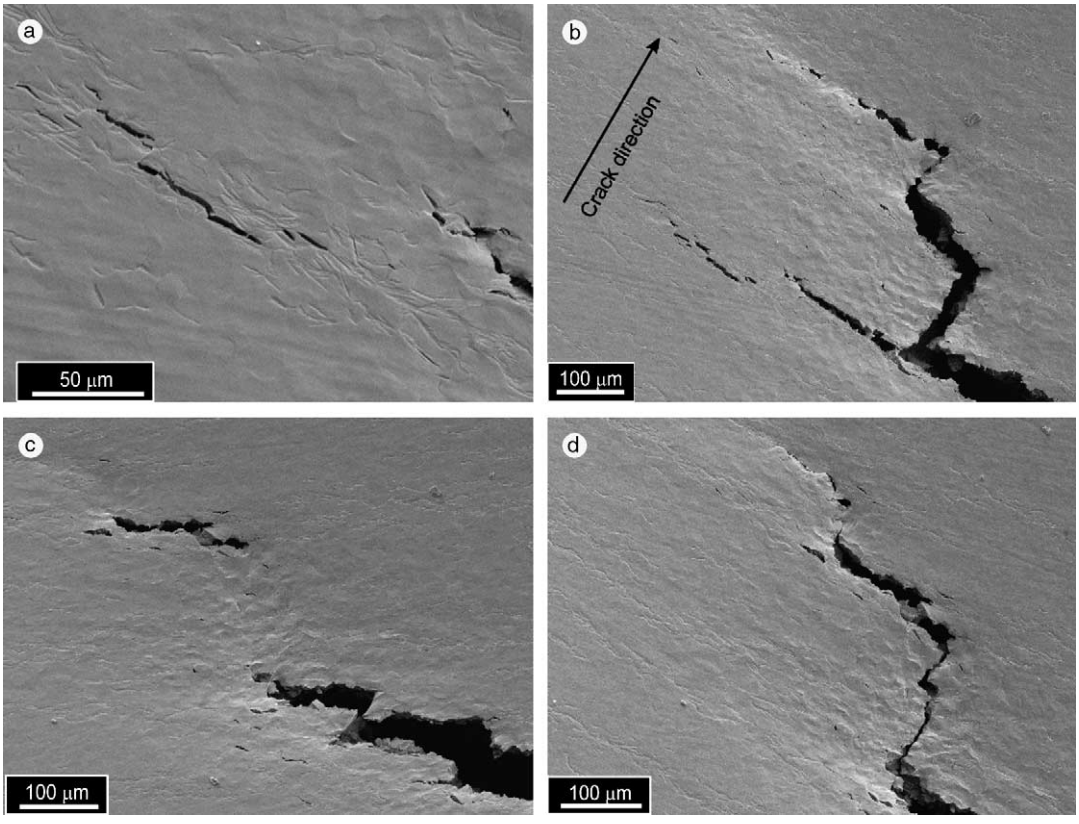

Fig. 12. Crack growth by the hydrides normal oriented respect to the initial crack direction, specimen with 1400 ppm.

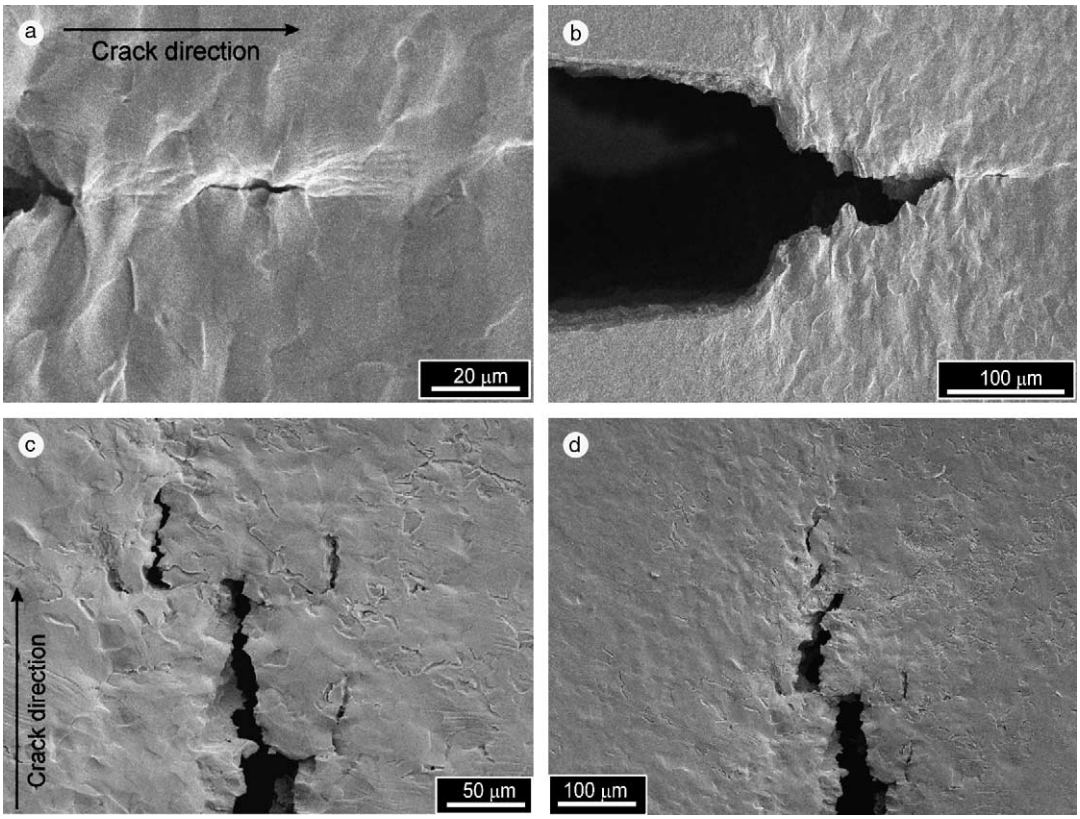

Fig. 13. Crack growth by hydrides parallels to the crack direction, specimen with 1300 ppm.

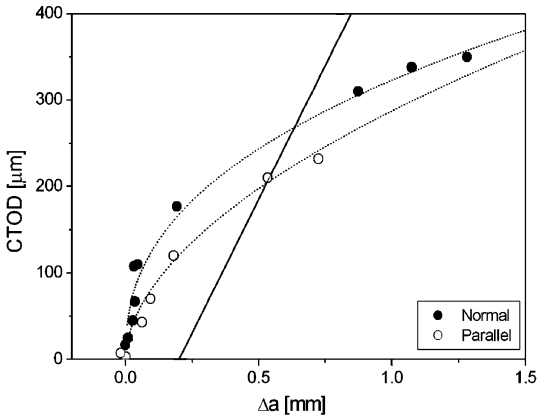

Fig. 14. CTOD vs. Δa curve for specimens with similar hydrogen content, with hydrides oriented parallel (1400 ppm) and normal (1300 ppm) to the pre-crack direction (the corresponding J_Q values are 180 and 238 kJ/m^2, respectively).

4. Conclusions

The effect of hydrogen content on the fracture toughness of Zry-4 was studied in this work by using a non-traditional technique that consists of testing small specimens inside the SEM. The method allows simultaneous load–displacement record and in situ observation and measurement of crack growth, hence facilitating the identification of those mechanisms acting during the crack initiation and propagation. Tests always showed macroscopic stable crack growth mechanism and the obtained resistance curves decreased as the hydrogen content was increased. Despite reduced sample size, a very good agreement with standard macro-CT results was also observed. The fracture toughness was also influenced by the orientation of the hydrides precipitates. Higher toughness values and fracture mechanisms with more plastic deformation were obtained for the precipitates normal to the crack path than for hydrides parallel to it. As the surface treatments helped to clearly identify grain boundaries and hydride precipitates, the crack growing mechanisms and the crack path throughout the hydride plateletes and the matrix were easily followed.

Acknowledgements

The authors thank Carlos Cotaro for his valuable help in characterization with SEM and Alejandro

Yawny and co-workers for the use of the testing device. The authors acknowledge the support from CNEA (Atomic Energy National Commission), CONICET (National Council of Scientific and Technological Research) and ANPCyT (PICT 99 BID/OC 1263).

References

[1] B.F. Kammenzind, D.G. Franklin, R.H. Peters, W.J. Duffin, ASTM STP 1295 (1996) 338.
[2] J.C. Clayton, ASTM STP 824 (1984) 572.
[3] F. Garzarolli, R.V. Jan, H. Stehle, Atom. Energy Rev. 17 (1979) 31.
[4] P. Vizcaíno, A.D. Banchik, J.P. Abriata, J. Nucl. Mater. 304 (2002) 96.
[5] M.P. Puls, Metall. Trans. A 19A (1988) 1507.
[6] C.E. Ells, J. Nucl. Mater. 28 (1968) 129.
[7] B.A. Cheadle, CRNL Report, CRNL-1208, 1974.
[8] A.A. Yawny, J.E. Perez Ipiña, J. Test. Eval. (in press).
[9] E.M. Castrodeza, F.L. Bastian, A. Yawny, J.E. Perez Ipiña, J. Compos. Mater. 36 (4) (2002) 387.
[10] E. Tenckhoff, ASTM STP 966 (1988).
[11] ASTM, 1999. Standard test method for measurement of fracture toughness, ASTM E 1820-99, Annual Book of ASTM Standards, vol. 03.01, 1999, p. 972.
[12] A. Yawny, J. Malarría, E. Soukup, M. Sade, Rev. Sci. Instrum. 68 (1997) 150.
[13] K.W. Lee, S.I. Hong, J. Alloys Compd. 346 (2002) 302.
[14] G. Bertolino, G. Meyer, J. Perez Ipiña, J. Alloys Compd. 330–332 (2002) 408.
[15] J.S. Dubey, S.L. Wadekar, R.N. Singh, T.K. Sinha, J.K. Chakravartty, J. Nucl. Mater. 264 (1999) 20.